Chapter 14
SOLE Project – Demonstration of a Multistatic and Multiband Coherent Radar Network

Giovanni Serafino, Salvatore Maresca, Filippo Scotti, Antonio Malacarne, Antonella Bogoni, Paolo Ghelfi, Leonardo Lembo, Carlo Noviello, Virginia Zamparelli, Gianfranco Fornaro, Eugenio Sansosti, Nicolas Torcheboeuf, and Steve Lecomte

Abstract The aim of the NATO-SPS SOLE project is demonstrating the feasibility and the high performance of a radar network thanks to photonics. Indeed, the coherence offered by photonics makes the proposed distributed radar system capable of an efficient implementation of MIMO processing and ISAR imaging, enhancing the performance in terms of resolution and precision. The advantage of a fully coherent, multistatic radar system here is experimentally proven by a 5-time cross-range resolution enhancement thanks to MIMO processing, and in an efficient focusing in ISAR imaging.

Keywords Photonic radar · MIMO radar · ISAR imaging · Mode-locked lasers

14.1 Introduction

Recently, distributed radar systems have attracted high interest, as a mean to increase the level of system performance, e.g. applying the multiple input-multiple output (MIMO) paradigm [1, 2]. Yet, practical implementations have been rarely

G. Serafino · S. Maresca · F. Scotti · A. Malacarne
TeCIP Institute, Scuola Superiore Sant'Anna, Pisa, Italy

A. Bogoni (✉) · P. Ghelfi
PNTLab, Consorzio Nazionale Interuniversitario per le Telecomunicazioni (CNIT), Pisa, Italy
e-mail: antonella.bogoni@santannapisa.it

L. Lembo
Vallauri Institute, Centro di Supporto e Sperimentazione Navale (CSSN), Livorno, Italy

C. Noviello · V. Zamparelli · G. Fornaro · E. Sansosti
Istituto per il Rilevamento Elettromagnetico dell'Ambiente (CNR-IREA), Napoli, Italy

N. Torcheboeuf · S. Lecomte
Centre Suisse d'Electronique et de Microtechnique (CSEM), Neuchâtel, Switzerland

C. Palestini (ed.), *Advanced Technologies for Security Applications*, NATO Science for Peace and Security Series B: Physics and Biophysics,
https://doi.org/10.1007/978-94-024-2021-0_14

proposed, since the attained complexity of such systems was too high, compared to the advantages granted by this kind of solutions. Indeed, to exploit all the advantages they offer, radar networks require a high phase coherence among all the nodes [3], which is very hard to obtain with classical electronic technology. In many cases, signal post-processing techniques can be applied to reconstruct the needed coherence; however, this usually translates in a huge, barely affordable computational complexity, which does not represent only a waste of resources, but can also introduce long time delays, making real-time applications of radar networks unattractive. However, in the last two decades, photonics started penetrating radio frequency (RF) remote sensing systems [4, 5]. Thanks to the guaranteed phase coherence in signal generation [6] and distribution [7], photonics introduces the possibility of going beyond the original concept of stand-alone radar, enabling the feasibility of distributed radars, without requiring an exaggerated increase of the computational load.

The "multiStatic & multiband cOherent radar fLeet for border sEcurity" (SOLE) project aims at the realization of a demonstrator of a 3 transmitters (TXs) by 3 receivers (RXs) full-functional radar network for surveillance purposes, based on the coherent multi-static approach, leveraging on the intrinsic high level of coherence of photonics [8]. The proposed system benefits from the MIMO approach, enhancing the cross-range resolution [2], and enabling the possibility of implementing high-performance imaging algorithms [9]. To this aim, suitable data processing techniques are considered, as well as algorithms for multistatic inverse synthetic aperture radar (ISAR) applications, to obtain a radar with enhanced sensitivity and precision.

Here, we report on the experimental activities for a first validation of the architecture of the proposed system and the related processing. In a campaign of in-field measurements, we tested a preliminary version of the photonic, multistatic coherent radar network, with 2 TXs and 2 RXs, applying MIMO and ISAR processing to the acquired data, showing the increased performance granted by the photonics in a radar network.

14.2 The SOLE Project Radar Network Architecture

The proposed distributed radar system architecture is composed by a central unit (CU) and three sensor peripherals (SPs). The CU and the SPs are connected by means of single mode fiber (SMF) spans. The architecture of the CU is shown in Fig. 14.1a. It can be ideally divided in a transmit (top) and receive (bottom) section. The master optical oscillator is implemented by a mode-locked laser (MLL) with a 600-MHz pulse repetition rate. The transmit section is equipped with three Mach-Zehnder modulators (MZMs) that will operate electro-optical (E/O) conversion of the radar waveforms generated at intermediate frequency (IF) by the digital-to-analog converters (DACs). The employed optical carriers are extracted from the

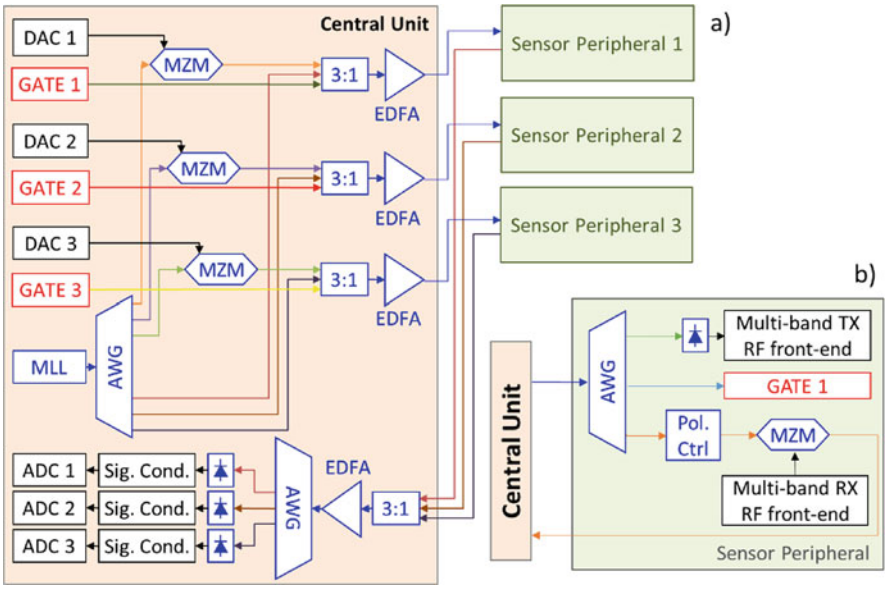

Fig. 14.1 Detailed description (**a**) of the photonics-assisted CU of the SOLE radar network and (**b**) of the structure of the SPs

MLL, which represents the system optical clock, by an arrayed waveguide grating (AWG). The optical carrier is fed into the MZM, where it is electro-optically modulated by the IF signal. The AWG extracts from the MLL spectrum also one line for each SP, that will be employed by the RXs as optical carrier for the E/O conversion of the received radar echoes: for this reason, it is sent unmodulated to the SP. Moreover, a gate to control the transmit and receive operations inside the SPs is generated and converted to the optical domain exploiting the direct modulation of a continuous-wave laser. A 3:1 optical coupler aggregates the radar waveforms converted to the optical domain, the unmodulated optical carrier from the MLL and the E/O converted gate to drive the operation of the SP. These three optical signals are transmitted together through the SMF to one of the SPs, after amplification by an Erbium-doped fiber amplifier (EDFA). This structure is repeated thrice inside the CU, once for each SP.

In the CU section dedicated to the received signals, there is another 3:1 coupler collecting the optical signals coming from the RXs of the three SPs, on three different wavelengths. After an EDFA, another AWG splits the three signals at the input of three photodetectors (PD) for the opto-electrical (O/E) conversion of the radar waveform to base band (BB). The PD outputs, after signal conditioning, are separately digitized by three analog-to-digital converters (ADCs). The SOLE photonic MIMO radar demonstrator will operate on S and X band. Transmission and reception orthogonality between the SPs will be obtained thanks to time division

multiplexing (TDM), i.e. each SP will transmit and receive in different moments. The coordination in time of the SPs operations is achieved thanks to the gate signals.

The scheme of the structure of a sensor peripheral is shown in Fig. 14.1b. The three optical signal coming from the CU are again separated by an AWG. The radar waveform is photodetected by a PD with a broad electrical BW. Then, among all the beating products at the output, the one centered at the desired RF frequencies in X and S band are selected by suitable electrical filters inside the front-end, before amplification and transmission by a wide-band antenna. The received radar echoes gathered by the antenna are fed into the electrical input of a MZM and E/O converted, modulating the mode coming from the MLL. An automatic polarization controller keeps the polarization of the incoming MLL mode aligned with the input polarization axis of the MZM, to optimize the power losses. The MZM output is transmitted on the SMF to the CU, where it is received and acquired.

14.3 The Optical Master Clock

In order to optically generate and distribute the signals in the photonics-assisted radar concept, it is advantageous to start with a system clock in the optical domain instead of an electrical clock (quartz, dielectric resonant oscillator, etc.) involving E/O conversion. MLLs are oscillators with unique phase noise purity: the physics of such oscillators, and in particular for those based on a diode-pumped solid-state laser architecture, allows for unmatched phase purity. Since optical fibers and telecom components are used in the radar system, a MLL emitting in a telecom band is necessary. For this purpose, the 600-MHz repetition rate solid-state laser based on Er:Yb:glass gain medium and passively mode-locked with a semiconductor saturable absorber mirror has been realized. A laboratory version of this laser, shown in Fig. 14.2a, emits about 80 mW of output power with soliton pulses of spectral full width half maximum of 12.5 nm (corresponding to a duration of 204 fs) and centered at 1561 nm. The fundamental line of the MLL electrical spectrum, at 600 MHz, is

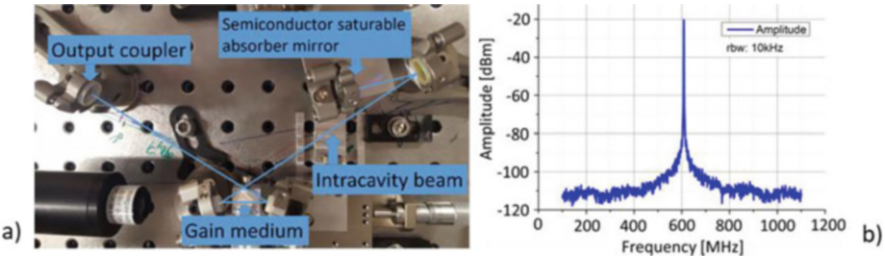

Fig. 14.2 (**a**) Laboratory version of the 600 MHz soliton MLL. The blue lines correspond to the beam path in the standing-wave cavity; (**b**) Lower-frequency component of the electrical spectrum of the MLL, with a spectral purity of around 70 dB

reported in Fig. 14.2b, showing the high spectral purity of such tone, around 70 dB. Now emphasis is made on the packaging of such a laser for reliable and long-term operation.

14.4 Processing and Target Detection

14.4.1 The MIMO Radar Concept and Processing

Unlike generic multistatic radars, MIMO radars are characterized by a high level of coordination between the central and the remote nodes; this unique feature allows to jointly process at the central node the multiple data streams with no need of local pre-processing at the remote nodes [1]. For this reason, they are particularly suitable for surveillance applications. In particular, MIMO radars with widely-separated antennas have the ability to observe the target from different aspect angles [1]. This offers many advantages, like the "super-resolution", i.e. the ability of enhancing the cross-range resolution beyond the limit imposed by the antenna aperture and even higher than the in-range resolution.

Following the general radar signal processing scheme [10], here we will focus our interest mainly on the MIMO fusion and target imaging strategies. In the case of a radar network with M TXs and N RXs, the CU employs N ADCs to digitize the received signals, which are the combinations of the M echo signals from each TXs. With the subscript k, l we indicate the generic radar employing the generic kth TX and lth RX pair, with $k = 1, \ldots, M$ and $l = 1, \ldots, N$. In the signal conditioning stage [10], the N digitized data streams are split into the $M \times N$ individual bistatic channels for data processing. After conditioning, the BB equivalent of the signal received by the lth RX is [1]:

$$r_{k,l}(t) = a_{k,l} \cdot s_k \left(t - \tau_{k,l}\right) e^{j[\theta(t-\tau_{k,l})-\theta(t)]} + n_{k,l}(t), \tag{14.1}$$

where $s_k(t)$ is the signal transmitted by the kth RX, $a_{k,\,l}$ is an amplitude factor, while $\tau_{k,\,l}$ is the time delay proportional to the bistatic distance, being function of the target location (x, y) and the TX/RX positions in the Cartesian plane. The term $n_{k,\,l}(t)$ is modelled as an additive white Gaussian noise stochastic process, while the phase noise $\theta(t)$ models the phase instability caused by the oscillator. When the angular jitter is less than 0.1 rad [3], the coherent MIMO log-likelihood function can be calculated as [1]:

$$\Lambda(t) = a \left| \sum_{k=1}^{M} \sum_{l=1}^{N} e^{-j2\pi f_{IF} \tau_{k,l}} \int r^*_{k,l}(t) s_k \left(t - \tau_{k,l}\right) dt \right| + b. \tag{14.2}$$

For each possible target location (x, y) in the monitored space, the statistic $\Lambda(t)$ is computed determining the MN correlations between the received and transmitted

signals, while the phase term $e^{-j2\pi f_{IF}\tau_{k,l}}$ compensates the phase shift due to time delay $\tau_{k,l}$. Finally, all the *MN* correlation contributes are summed together coherently. This phase compensation (i.e. coherent MIMO processing) is feasible only when the system architecture can ensure time/phase synchronization. This is the case of the proposed photonic radar network, which employs the same optical oscillator, with very low phase noise [6], for both signal generation and detection. In fact, the temporal jitter of the considered system is in the order of 10^{-12} s, while the angular jitter is in the order of 0.01 rad [8], far better than the operative limit [3].

14.4.2 Multistatic ISAR Processing

ISAR imaging founds on the possibility to gather information of the target from slightly different angular positions by exploiting the relative motion between the sensor and the target. The backscatter echoes from the targets need to be coherently processed to obtain high-resolution images in the cross range direction [9]. Notwithstanding, the target motion which is necessary to produce the angular imaging variation, is also typically responsible of the presence of phase variation that, if not properly compensated, would be source of large defocusing. The target motion shall be, generally, estimated directly from the data and then properly compensated. It can be shown that, for a target characterized by a uniform motion, the bistatic delay can be expressed in the form:

$$\tau_{k,l}(t) = \frac{2R_{k,l}(t)}{c}, \quad R_{k,l}(t) = R_{0kl} + \gamma_{k,l}t + \delta_{k,l}t^2 \tag{14.3}$$

with $\gamma_{k,l}$ and $\delta_{k,l}$ being parameters proportional to the Doppler centroid and Doppler rate associated to each sensor pair (k,l); in fact, the influence of the Doppler Centroid is mandatory to separate the moving target from the static clutter, and, high value of the Doppler rate allows to achieve sufficient system focusing capabilities, respectively. The block diagram in Fig. 14.3 describes the processing implemented to perform the focusing of ISAR data for either monostatic or bistatic configurations. Core of the procedure is the target motion estimation and compensation, which is based on Doppler analysis. Following this step, an inverse Fast Fourier Transform

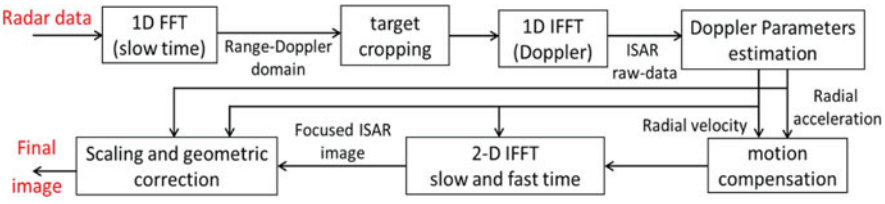

Fig. 14.3 Block diagram of the focusing procedure for monostatic and bistatic ISAR data

(IFFT) is carried out to obtain the focused image: eventually, a scaling is performed in the cross range direction to achieve the final pixel size.

14.5 Experimental Activities and Results

To validate the approach proposed in SOLE project, we present a preliminary test of the multi-static coherent radar network in a real outdoor scenario. Two measurement campaigns have been carried on: the first with extended targets, to validate the imaging capability of the system; the second, with multiple small, closely-spaced targets to demonstrate the attained enhanced resolution. It is important to remark that the system always worked in X band but, between the first and the second field trial, it underwent an upgrade of the employed BW from 20 to 100 MHz.

The scheme of the tested radar network [8] is depicted in Fig. 14.4a. It is composed of 2 TXs $\times$ 2 RXs, connected to the CU through SMF, working as explained in Sect. 14.2. The MLL enables generating RF carriers with extremely low phase noise, upon the O/E conversion of the MLL modes in a PD [6], thus implementing high-quality RF up-conversion and down-conversion. Moreover, exploiting a single MLL for these operations ensures a perfect synchronization of the SPs and maintains the coherence of the signals, which is the most crucial issue in coherent MIMO radars. The radar signal, a linear frequency-modulated upsweep chirp pulsed signal with 100 ns duration, pulse repetition interval (PRI) of 50 μs and BW B, is digitally generated at $f_{\mathrm{IF}} = 100$ MHz, whereas the RF output carrier frequency is $f_{\mathrm{RF}} = 9.7$ GHz. The large MLL optical spectrum ensures high efficiency, and the wide electrical BW of MZMs and PDs allows for the flexible management of RF signals up to several tens of GHz [6]. The employed antennas at the TXs and RXs are ultra-wideband horn antennas with about 50° half-power beam width (HPBW) aperture and 12 dBi maximum gain. The output power of each antenna was about 100 mW. The optical delay line (ODL) depicted in Fig. 14.4a, consisting of a 1 km-long SMF spool inserted before the TX of SP2, implements the TDM between the two SPs. The detected echoes received by the SPs are sent to the CU, where they are down-converted, low-pass filtered, fed into a two-channel acquisition system and digitized by an ADC at 400 MS/s per channel. An aerial picture of the out-door experimental setup, taken by one of the drones carrying a target, is reported in Fig. 14.4b, showing the geometry of the radar network. The four horn antennas were aligned along a 21-m baseline.

The multistatic ISAR processing, based on Doppler Parameter Estimation Algorithm described in Sect. 14.4.2, has been adopted for testing the imaging capability of the photonic radar network on moving targets. Experiments on extended targets have been conducted employing a single TX and both RXs with $B = 20$ MHz, with a range resolution of 15 m, with an observation interval of 0.1 s which limited the Doppler resolution to 10 Hz. The chosen targets were airplanes taking off in the proximity of the building. In Fig. 14.5 are shown the images of the target before (a, c) and after (b, d) the focusing in the Range-Cross range domain, for the RX1 (a, b)

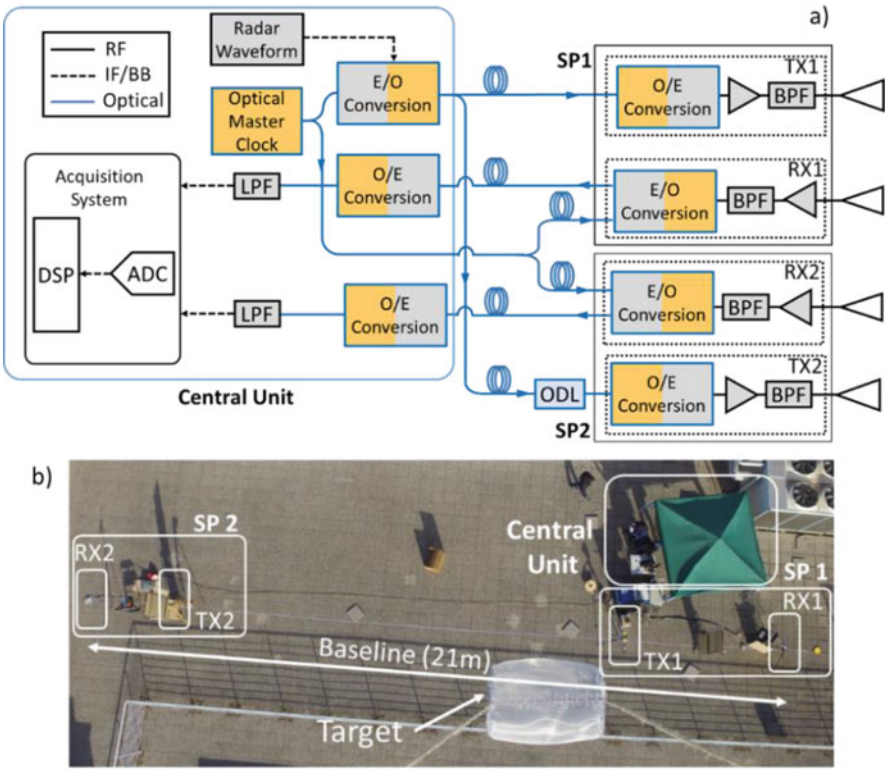

Fig. 14.4 (**a**) Architecture of the proposed Photonic Radar Network. *DSP* Digital Signal Processing, *BPF* Band-Pass Filter, *LPF* Band-Pass Filter. (**b**) Aerial picture of the test field, taken by one of the drones carrying the targets. The target is the metal net cylinder hanging from the drone

and RX2 (c, d). The selected target is moving at radial velocity of about 130 km/h, at a distance from the baseline of around 770 m. Although it is difficult to identify the shape of the airplane, the visual inspection demonstrates the capability of the algorithm to achieve well focused images, despite the short acquisition time, thanks to the stability of the optically generated and distributed signals.

Table 14.1 reports typical quality parameters to evaluate imaging performances for both RXs. As apparent from the results, all the parameters improve after the application of the ISAR imaging algorithm, thus confirming the capability of the system to guarantee good performances. Even though the analysis were carried out on a premature version of the radar system which is not tuned to ISAR imaging, the achieved results are rather promising.

In the second measurements set, carried out employing all TXs and RXs, with a BW $B = 100$ MHz, the two cooperative targets consisted of two cylinders, with 17 cm radius and 50 cm height, made of a tight-mesh metal net and hanging from two mini-drones hovering above the baseline. The two targets were always kept at a

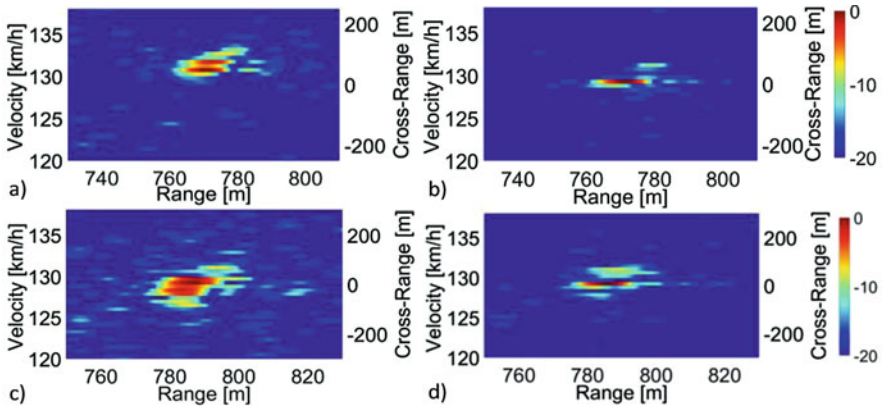

Fig. 14.5 Unfocused (**a**, **c**) vs focused (**b**, **d**) ISAR images of a target took in the first set of measurements, by RX1 (**a**, **b**) and RX2 (**c**, **d**)

Table 14.1 Quality imaging parameters

	RX1			RX2		
Parameters	Unfocused	Focused	Relative	Unfocused	Focused	Relative
Contrast	1.06	1.12	+5.81%	1.02	1.09	+6.54%
Entropy	7.43	7.09	−4.66%	7.61	7.31	−3.99%
Peak	0.30	0.40	+34.96	0.23	0.37	+56.56
Sharpness	0.22	0.37	+69.90%	0.16	0.35	+124.71%

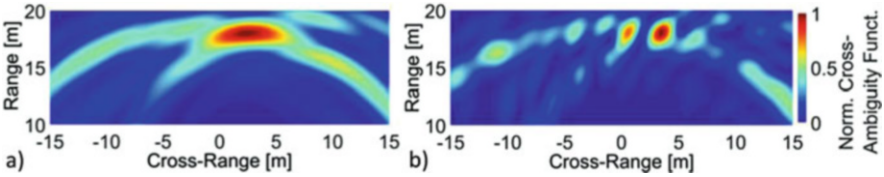

Fig. 14.6 Normalized cross-ambiguity function as processing output of the MIMO detection in the second set of measurements with two closely-spaced targets. (**a**) Non-coherent MIMO with two unresolved targets; (**b**) coherent MIMO where the targets are clearly distinguishable

distance of around 3 m from each other, at 18 m above the baseline. The axes of the cylinders were perpendicular to the baseline, to enhance the radar cross-section seen from the antennas. As we can observe in Fig. 14.6a, the two targets are too close to be correctly separated in the cross-range with a MIMO non-coherent processing. Indeed, being the in-range distance from the baseline of the two targets 18 m, and given the antenna HPBW ~50°, the expected monostatic cross-range resolution is 15.7 m. Figure 14.6b, instead, depicts the output of the coherent MIMO processing. Here, the two targets are correctly separated in cross-range, around 3 m apart from each other, demonstrating a cross-range resolution improvement by a factor of 5.

14.6 Conclusions and Future Works

A coherent MIMO radar network demonstrator based on photonic technology has been presented and tested in a real outdoor environment. The capability of the distributed system, specifically tailored to real-time surveillance applications, of performing MIMO processing and ISAR imaging have been demonstrated. Two cooperative closely-spaced targets have been successfully resolved in cross-range by applying coherent MIMO processing, which enhanced the resolution by 5 times. The superiority of such an approach compared with the non-coherent approach is apparent, demonstrating the benefits of the photonics-assisted proposed architecture. Moreover, the efficiency of ISAR processing by this distributed radar network on an extended target, represented by an airplane, have been shown. The here-presented results should be considered as a starting point: further field trials are planned in the next future with an extended architecture, with one more SP and working at the same time in X and S band, with much more largely distributed antennas, as the final goal of the SOLE project.

References

1. Haimovich AM et al (2008) MIMO radar with widely separated antennas. IEEE Signal Process Mag 25(1):116–129
2. Lehmann NH et al (2006) High resolution capabilities of MIMO radar. 40th IEEE Asilomar conference on signals system and computers, Pacific Groove, USA
3. Pasya I et al (2013) Detection performance of M-sequence-based MIMO radar systems considering phase Jitter effects. IEEE phased array systems & technology symposium
4. Ghelfi P et al (2014) A fully photonics-based coherent radar system. Nature 507:341–345
5. Laghezza F et al (2015) Field evaluation of a photonics-based radar system in a maritime environment compared to a reference commercial sensor. IET Radar Sonar Navig 9(8):1040–1046
6. Serafino G et al (2011) Phase and amplitude stability of EHF-band radar carriers generated from an active mode-locked laser. J Lightwave Technol 29(23):3551–3559
7. Williams P et al (2008) High-stability transfer of an optical frequency over long fiber-optic links. J Opt Soc Am B 25:1284–1293
8. Lembo L et al (2019) In-field demonstration of a photonic coherent MIMO distributed radar network. IEEE radar conference 2019, Boston
9. Noviello C et al (2017) Fast and accurate ISAR focusing based on a Doppler parameter estimation algorithm. IEEE Geosci Remote Sens Lett 14(3):349–353
10. Richards GA (2014) Fundamentals of radar signal processing, 2nd edn. McGraw-Hill, New York